

A 15 GSa/s, 1.5 GHz Bandwidth Waveform Digitizing ASIC

Eric Oberla^{a,*}, Jean-Francois Genat^{a,1}, Hervé Grabas^{a,2}, Henry Frisch^a, Kurtis Nishimura^{b,3}, Gary Varner^b

^a*Enrico Fermi Institute, University of Chicago; 5640 S. Ellis Ave., Chicago IL, 60637*

^b*University of Hawai'i at Manoa; Watanabe Hall, 2505 Correa Rd., Honolulu HA*

Abstract

The PSEC4 custom integrated circuit was designed for the recording of fast waveforms for use in large-area time-of-flight detector systems. The ASIC has been fabricated using the IBM-8RF 0.13 μm CMOS process. On each of 6 analog channels, PSEC4 employs a switched capacitor array (SCA) 256 samples deep, a ramp-compare ADC with 10.5 bits of DC dynamic range, and a serial data readout with the capability of region-of-interest windowing to reduce dead time. The sampling rate can be adjusted between 4 and 15 Gigasamples/second [GSa/s] on all channels and is servo-controlled on-chip with a low-jitter delay-locked loop (DLL). The input signals are passively coupled on-chip with a -3 dB analog bandwidth of 1.5 GHz. The power consumption in quiescent sampling mode is less than 50 mW/chip; at a sustained trigger and readout rate of 50 kHz the chip draws 100 mW. After fixed-pattern pedestal subtraction, the uncorrected integral non-linearity is 0.15% over an 750 mV dynamic range. With a linearity correction, a full 1 V signal voltage range is available. The sampling timebase has a fixed-pattern non-linearity with an RMS of 13%, which can be corrected for precision waveform feature extraction and timing.

Keywords:

Waveform sampling, ASIC, Integrated Circuit, Analog-to-Digital, Switched Capacitor Array, Time-of-Flight

1. Introduction

We describe the design and performance of PSEC4, a ≥ 10 Gigasample/second [GSa/s] waveform sampling and digitizing Application Specific Integrated Circuit (ASIC) fabricated in the IBM-8RF 0.13 μm complementary metal-oxide-semiconductor (CMOS) technology. This compact ‘oscilloscope-on-a-chip’ is designed for the recording of radio-frequency (RF) transient waveforms with signal bandwidths between 100 MHz and 1.5 GHz.

*Corresponding author

Email address: ejo@uchicago.edu (Eric Oberla)

¹Present address, LPNHE, CNRS/IN2P3, Universités Pierre et Marie Curie and Denis Diderot, T12 RC, 4 Place Jussieu 75252 Paris CEDEX 05, France

²Present address, CEA/IRFU/SEDI; CEN Saclay-Bat141 F-91191 Gif-sur-Yvette CEDEX, France

³Present address, SLAC National Accelerator Laboratory, 2575 Sand Hill Road, Menlo Park, CA 94025

7 *1.1. Background*

8 The detection of discrete photons and high-energy particles is the basis of a wide range of commercial
9 and scientific applications. In many of these applications, the relative arrival time of an incident photon
10 or particle is best measured by extracting features from the full waveform at the detector output [1, 2].
11 Additional benefits of front-end waveform sampling include the detection of pile-up events and the ability
12 to filter noise or poorly formed pulses.

13 For recording ‘snapshots’ of transient waveforms, switched capacitor array (SCA) analog memories can
14 be used to sample a limited time-window at a relatively high rate, but with a latency-cost of a slower readout
15 speed [3, 4]. These devices are well suited for triggered-event applications, as in many high energy physics
16 experiments, in which some dead-time on each channel is acceptable. With modern CMOS integrated circuit
17 design, these SCA sampling chips can be compact, low power, and have a relatively low cost per channel [4].

18 Over the last decade, sampling rates in SCA waveform sampling ASICs have been pushed to several
19 GSa/s with analog bandwidths of several hundred MHz up to ~ 1 GHz [5, 6]. As a scalable front-end
20 readout option coupled with the advantages of waveform sampling, these ASICs have been used in a wide
21 range of experiments; such as high-energy physics colliders [6], gamma-ray astronomy [7, 8], high-energy
22 neutrino detection [9, 10], and rare decay searches [11, 12].

23 *1.2. Motivation*

24 A natural extension to the existing waveform sampling ASICs is to push design parameters that are
25 inherently fabrication-technology limited. Parameters such as sampling rate and analog bandwidth are of
26 particular interest considering the fast risetimes ($\tau_r \sim 60 - 500$ ps) and pulse widths (FWHM ~ 200 ps - 1 ns)
27 of commercially available and novel technologies of micro-channel plate (MCP) and silicon photomultipli-
28 ers [13, 14, 15]. These and other fast photo-optical or RF devices require electronics matched to the speed
29 of the signals.

30 The timing resolution of discrete waveform sampling is intuitively dependent on three primary factors
31 as described by Ritt⁴ [16]:

$$\sigma_t \propto \frac{\tau_r}{(SNR)\sqrt{N_{samples}}} \quad (1)$$

32 where SNR is the signal-to-noise ratio of the pulse, τ_r is the 10-90% rise-time of the pulse, and $N_{samples}$
33 is the number of independent samples on the rising edge within time τ_r . The motivation for oversampling

⁴Assuming Shannon-Nyquist is fulfilled

34 above the Nyquist limit is that errors due to uncorrelated noise, caused both by random time jitter and
35 charge fluctuations, are reduced by increasing the rising-edge sample size. Accordingly, in order to preserve
36 the timing properties of analog signals from a fast detector, the waveform recording electronics should 1) be
37 low-noise, 2) match the signal bandwidth, and 3) have a fast sampling rate relative to the signal rise-time.

38 *1.3. Towards 0.13 μm CMOS*

39 The well-known advantages of reduced transistor feature size include higher clock speeds, greater circuit
40 density, lower parasitic capacitances, and lower power dissipation per circuit [17]. The sampling rate and
41 analog bandwidth of waveform sampling ASICs, which depend on clock speeds, parasitic capacitances, and
42 interconnect lengths, are directly enhanced by moving to a smaller CMOS technology. Designing in a smaller
43 technology also allows clocking of an on-chip analog-to-digital converter (ADC) at a faster rate, reducing
44 the chip dead-time.

45 With the advantages of reduced transistor feature sizes also comes increasingly challenging analog design
46 issues. One issue is the increase of leakage current. Leakage is enhanced by decreased source-drain channel
47 lengths, causing subthreshold leakage ($V_{GS} < V_{TH}$), and decreased gate-oxide thickness, which promotes
48 gate-oxide tunneling [18]. Effects of leakage include increased quiescent power dissipation and potential
49 non-linear effects when storing analog voltages.

50 Another design issue of deeper sub-micron technologies is the reduced dynamic range [18]. The available
51 voltage range is given by $(V_{DD}-V_{TH})$, where V_{DD} is the supply voltage and V_{TH} is the threshold, or ‘turn-
52 on’, voltage for a given transistor. For technologies above 0.1 μm , the $(V_{DD}-V_{TH})$ range is decreased with
53 downscaled feature sizes to reduce high-field effects in the gate-oxide [18]. In the 0.13 μm CMOS process,
54 the supply voltage V_{DD} is 1.2 V and the values of V_{TH} range from 0.42 V for a minimum-size transistor
55 (gate length 120 nm) to roughly 0.2 V for a large transistor (5 μm) [19, 20].

56 The potential of waveform sampling design in 0.13 μm CMOS was shown with two previous ASICs. A
57 waveform sampling prototype, PSEC3, achieved a sampling rate of 15 GSa/s and showed the possibility of
58 analog bandwidths above 1 GHz [21]. Leakage and dynamic range studies were also performed with this
59 chip. In a separate 0.13 μm ASIC, fabricated as a test-structure chip called CHAMP, a 25 GSa/s sampling
60 rate rate was achieved using low V_{TH} transistors [22]. The performance and limitations of these chips led
61 to the optimized design of the PSEC4 waveform digitizing ASIC. The fabricated PSEC4 die is shown in
62 Figure 1.

63 In this paper, we describe the PSEC4 architecture (§2), and experimental performance (§3).

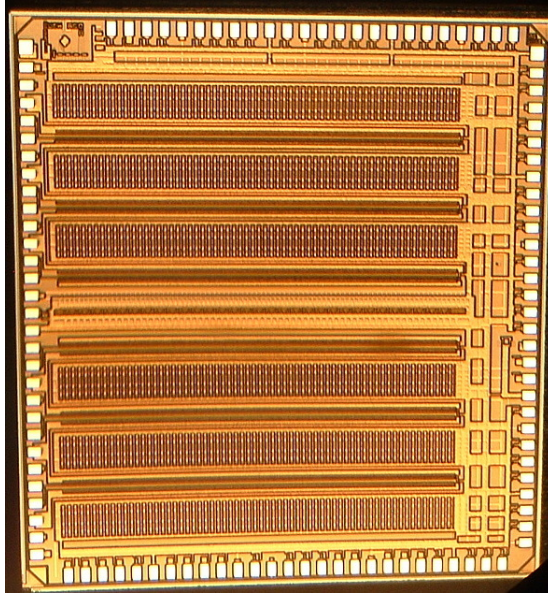


Figure 1: Photograph of the fabricated PSEC4 die. The chip dimensions are $4 \times 4.2 \text{ mm}^2$.

2. Architecture

An overview of the PSEC4 architecture and functionality is shown in Figure 2. A PSEC4 channel is a linear array of 256 sample points and a threshold-level trigger discriminator. Each sample point in the array is made from a switched capacitor sampling cell and an integrated ADC circuit as shown in Figure 3.

To operate the chip, a field-programmable gate array (FPGA) is used to provide timing control, clock generation, readout addressing, data management, and general configurations to the ASIC. Several analog voltage controls are also required for operation, and are provided by commercial digital-to-analog converter (DAC) chips.

Further details of the chip architecture, including timing generation (§2.1) sampling and triggering (§2.2), analog-to-digital conversion (§2.3), and data readout (§2.4), are outlined in the following sections.

2.1. Timing Generation

The sampling signals are generated with a 256-stage Voltage-Controlled Delay Line (VCDL), in which the individual stage time delay is adjustable by two complementary voltage controls. There is a single VCDL that distributes the timing signals to the entire chip. Each stage in the VCDL is an RC delay element made from a CMOS current-starved inverter. The inverse of the time delay between stages sets the sampling rate. Rates of up to 17.5 GSa/s are possible with PSEC4 as shown in Figure 4. When operating the VCDL

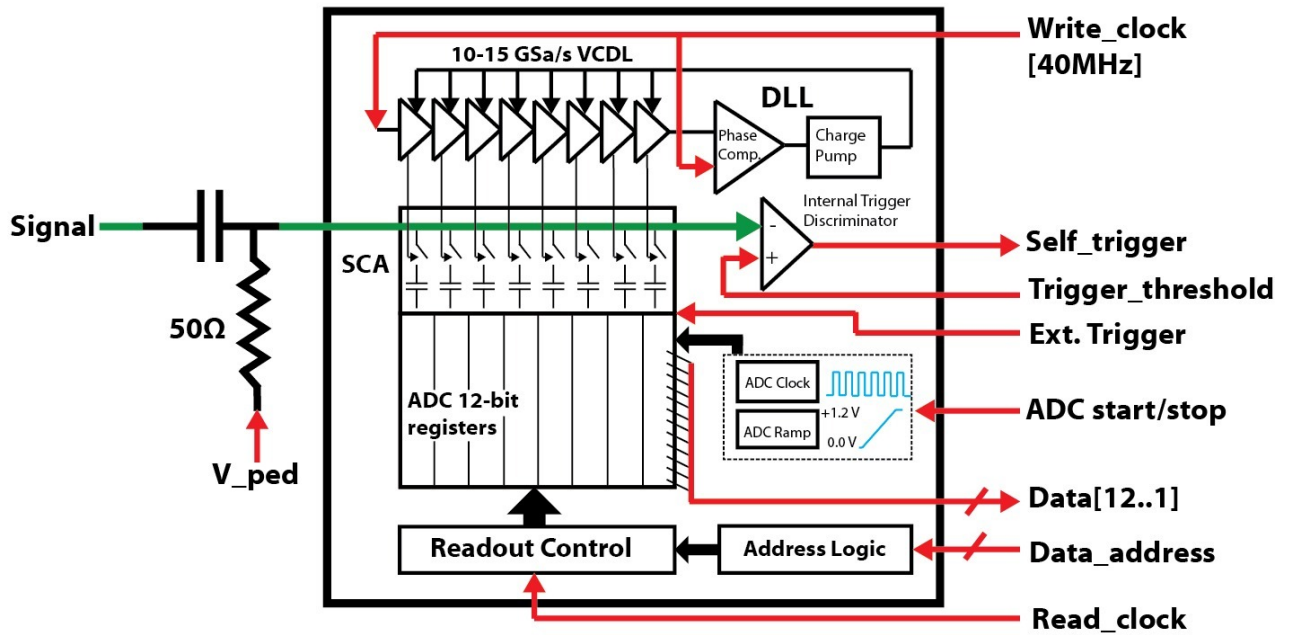


Figure 2: A block diagram of PSEC4 functionality. The RF-input signal is AC coupled and terminated in 50Ω off-chip. The digital signals (listed on right) are interfaced with an FPGA for PSEC4 control. A 40 MHz write clock is fed to the chip and up-converted to ~ 10 GSa/s with a 256-stage voltage-controlled delay line (VCDL). (For clarity, only 8 of the 256 cells and 1 of the 6 channels are illustrated). A ‘write strobe’ signal is sent from each stage of the VCDL to the corresponding sampling cell in each channel. The write strobe passes the VCDL-generated sampling rate to the sample-and-hold switches of each SCA cell. Each cell is made from a switched capacitor sampling cell and integrated ADC counter, as shown in Figure 3. The trigger signal ultimately comes from the FPGA, in which sampling on every channel is halted and all analog samples are digitized. The on-chip ramp-compare ADC is run with a global analog ramp generator and 1 GHz clock that are distributed to each cell. Once digitized, the addressed data are serially sent off-chip on a 12-bit bus clocked at up to 80 MHz.

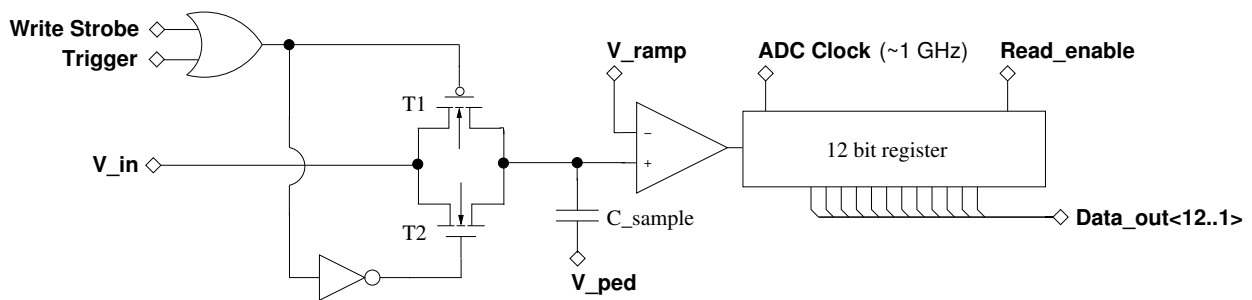


Figure 3: Simplified schematic of the ‘vertically integrated’ PSEC4 cell structure. The sampling cell input, V_{in} , is tied to the on-chip 50Ω input microstrip line. Transistors T1 and T2 form a dual-CMOS write switch that facilitates the sample-and-hold of V_{in} on C_{sample} , a 20 fF capacitance referenced to V_{ped} . The switch is toggled by the VCDL write strobe while sampling (Figure 2) or an ASIC-global trigger signal when an event is to be digitized. When the ADC is initiated, a global 0.0-1.2 V analog voltage ramp is sent to all comparators, which digitizes the voltage on C_{sample} using a fast ADC clock and 12-bit counter. To send the digital data off-chip, the register is addressed using $Read_enable$.

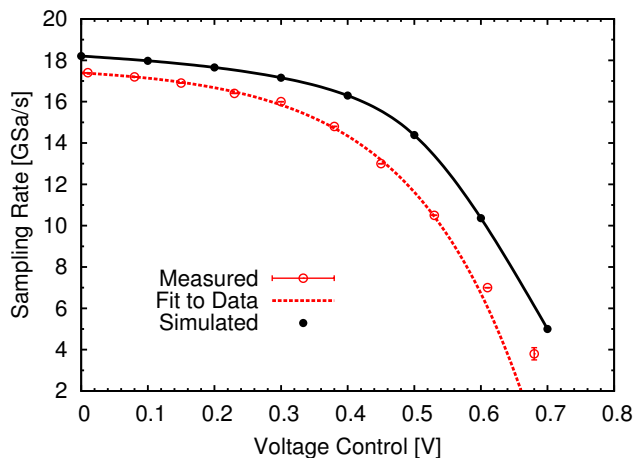


Figure 4: Sampling rate as a function of VCDL voltage control. Good agreement is shown between post layout simulation and actual values. Rates up to 17.5 GSa/s are achieved with the free-running PSEC4 VCDL.

80 without feedback, the control voltage is explicitly set and the sampling rate is approximately given by

$$18 - 0.3 e^{6 \cdot V_{control}} \text{ [GSa/s]}. \quad (2)$$

81 Typically, the servo-locking will be enabled and the VCDL is run as a delay-locked loop (DLL). In this case,
 82 the sampling rate is automatically set by the input write clock frequency. The stability of the sampling rate
 83 is negatively correlated with the slope magnitude as the VCDL becomes increasingly sensitive to noise. The
 84 slowest stable sampling rate is ~ 4 GSa/s.

85 A ‘write strobe’ signal is sent from each stage of the VCDL to the corresponding sampling cell in each
 86 channel. The write strobe passes the VCDL-generated sampling rate to the sample-and-hold switch of the
 87 cell as shown in Figure 3. To allow the sample cell enough time to fully charge or discharge when sampling,
 88 the write strobe is extended to a fixed duration of $8 \times$ the individual VCDL delay stage. In sampling mode,
 89 a ‘sampling block’ made of 8 adjacent SCA sampling cells continuously tracks the input signal.

90 To servo-control the VCDL at a specified sampling rate and to compensate for temperature effects and
 91 power supply variations, the VCDL can be delay-locked on chip. The VCDL forms a delay-locked loop
 92 (DLL) when this servo-controlled feedback is enabled. The servo-control circuit is made of a dual phase
 93 comparator and charge pump circuit to lock both the rising and falling edges of the write clock at a fixed
 94 one-cycle latency [23]. A loop-filter capacitor is installed externally to tune the DLL stability.

95 With this DLL architecture, a write clock with frequency f_{in} is provided to the chip, and the sampling is
96 started automatically after a locking time of several seconds. The nominal sampling rate in GSa/s is set by
97 $0.256 \cdot f_{in}$ [MHz], and the sampling buffer depth in nanoseconds is given by $10^3/f_{in}$ [MHz⁻¹]. A limitation
98 of the PSEC4 design is the relatively small recording depth at high sampling rates due to the buffer size of
99 256 samples.

100 2.2. Sampling and Triggering

101 A single-ended, 256-cell SCA was designed and implemented on each channel of PSEC4. Each sampling
102 cell circuit is made from a dual CMOS write switch and a metal-insulator-metal sampling capacitor as
103 shown in Figure 3. With layout parasitics, this capacitance is effectively 20 fF. During sampling, the write
104 switch is toggled by the write strobe from the VCDL. To record an event, an external trigger, typically
105 from an FPGA, overrides the sampling and opens all write switches, holding the analog voltages on the
106 capacitor for the ADC duration ($\leq 4 \mu\text{s}$). Triggering interrupts the sampling on every channel, and is held
107 until the selected data are digitized and read out. When triggered, the sampling is asynchronously halted.
108 This corrupts the voltage on the 7 sample cells that were in the process of sampling, reducing the effective
109 number of PSEC4 samples to 249.

110 The PSEC4 has the capability to output a threshold-level trigger bit on each channel. The internal
111 trigger is made from a fast comparator, which is referenced to an external threshold level, and digital logic
112 to latch and reset the trigger circuit. To form a PSEC4 trigger, the self-trigger bits are sent to the FPGA,
113 which returns a global trigger signal back to the chip. In the internal trigger mode, the trigger round-trip
114 time is 15-20 ns (depending on FPGA algorithm), which allows for the recording of a waveform before it is
115 overwritten at 10 GSa/s.

116 2.3. ADC

117 Digital conversion of the sampled waveforms is done on-chip with a single ramp-compare ADC that
118 is parallelized over the entire ASIC⁵. Each sample cell has a dedicated comparator and 12 bit counter as
119 shown in Figure 3. In this architecture, the comparison between each sampled voltage (V_{sample}) and a
120 global ramping voltage (V_{ramp}), controls the clock enable of a 12-bit counter. When $V_{ramp} > V_{sample}$, the
121 counter clocking is disabled, and the 12-bit word, which has been encoded by the ADC clock frequency and
122 the ramp duration below V_{sample} , is latched and ready for readout.

⁵An overview of this ADC architecture can be found in reference [24].

123 Embedded in each channel is a 5-stage ring oscillator that generates a fast digital ADC clock, adjustable
124 between 200 MHz and 1.4 GHz. The ADC conversion time, power consumption, and resolution may be
125 configured by adjusting the ramp slope or by tuning the ring oscillator frequency.

126 *2.4. Readout*

127 The serial data readout of the latched counter bits is performed using a shift register ‘token’ architecture,
128 in which a *read.enable* pulse is passed sequentially along the ADC counter array. To reduce the chip readout
129 latency, a limited selection of the 1536 counters in PSEC4 can be read out. Readout addressing is done
130 by selecting the channel number and a block of 64 cells. While not completely random access, this scheme
131 permits a considerable reduction in dead time. At a maximum rate of 80 MHz, the readout time is 0.8 μ s
132 per 64-cell block.

133 The readout latency is typically the largest contributor to the dead-time of the chip. The ADC conversion
134 time also adds up to 4 μ s of latency per triggered event. These two factors limit the sustained trigger rate
135 to \sim 200 kHz/channel or \sim 50 kHz/chip.

136 **3. Performance**

137 Measurements of the PSEC4 performance have been made with several chips on custom evaluation boards
138 shown in Figure 5. The sampling rate was fixed at a nominal rate of 10.24 GSa/s. Here we report on bench
139 measurements of linearity (§3.1), analog leakage (§3.2), noise (§3.3), power (§3.4), frequency response (§3.5),
140 sampling calibrations (§3.6), and waveform timing (§3.7). A summary table of the PSEC4 performance is
141 shown in §3.8.

142 *3.1. Linearity and Dynamic Range*

143 The signal voltage range is limited by the 1.2 V core voltage of the 0.13 μ m CMOS process [19]. To
144 enable the recording of signals with pedestal levels that exceed this range, the input is AC coupled and a
145 DC offset is added to the 50 Ω termination. This is shown in the Figure 2 block diagram, in which the DC
146 offset is designated by V_{ped} . The offset level is tuned to match the input signal voltage range to that of
147 PSEC4.

148 The PSEC4-channel response to a linear pedestal scan is shown in Figure 6. This is the average DC
149 response over all 256 cells in a channel. A signal voltage range of 1 V is shown, as input signals between
150 100 mV and 1.1 V are fully coded with 12 bits. An integral non-linearity (INL) of better than 0.15% is

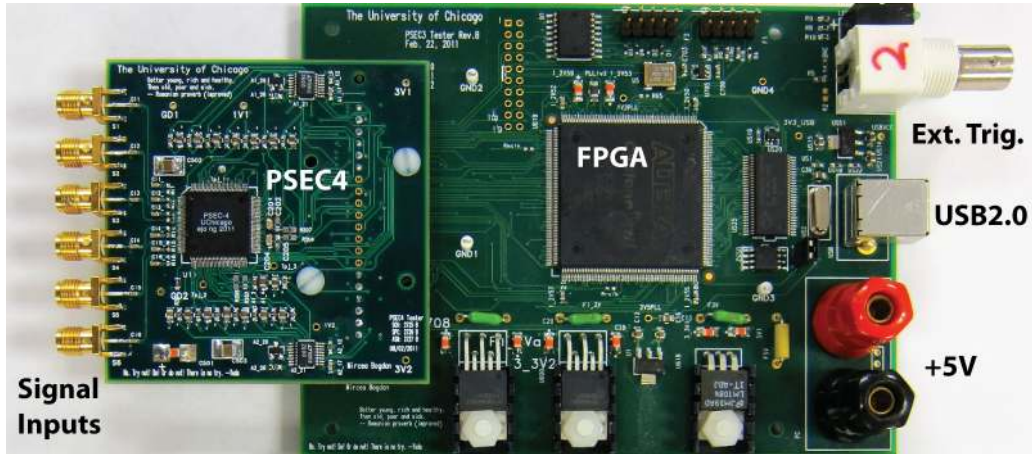


Figure 5: The PSEC4 evaluation board. The board uses a Cyclone III Altera FPGA (EP3C25Q240) and a USB 2.0 PC interface. Custom firmware and acquisition software were developed for overall board control. The board uses +5 V power and draws <math><400\text{ mA}</math>, either from a DC supply or the USB interface.

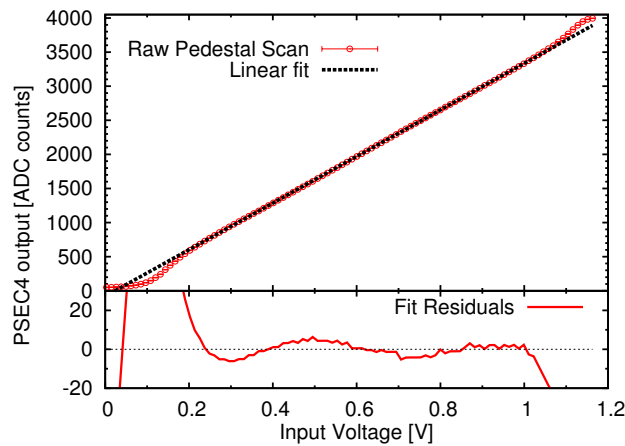


Figure 6: DC response of the device running in 12 bit mode. The data are an average response of all 256 cells from a single channel. The upper plot shows raw data (red points) and a linear fit over the the same dynamic range (dotted black line, slope of 4 counts/mV). The fit residuals are shown in the lower plot.

151 shown for most of that range. The non-linearity and limited DC signal range near the voltage rails are due
 152 to transistor threshold issues in the comparator circuit.

153 The DNL of this response, shown by the linear fit residuals in Figure 6, can be corrected by creating an
 154 ADC count-to-voltage look-up-table (LUT) that maps the input voltage to the PSEC4 output code. The
 155 raw PSEC4 data is converted to voltage and ‘linearized’ with a channel-averaged LUT.

156 Further linearity calibrations can be implemented to correct for cell-to-cell gain variations. A display of
 157 raw linearity scans over cells in a single channel is shown in Figure 7. After a cell pedestal subtraction, the

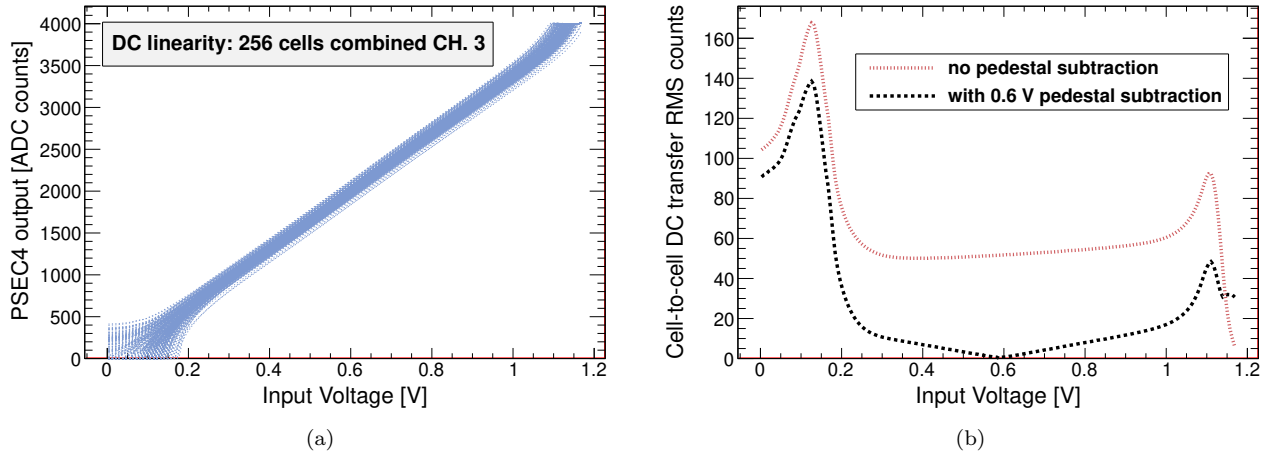


Figure 7: (a) Raw DC scans for all 256 PSEC4 cells on a single channel. (b) RMS spread in ADC counts scanned over input voltage on a PSEC4 channel. A mid-range pedestal subtraction on each cell reduces the RMS/mean spread to $\sim 1\%$ over an 0.8 V range

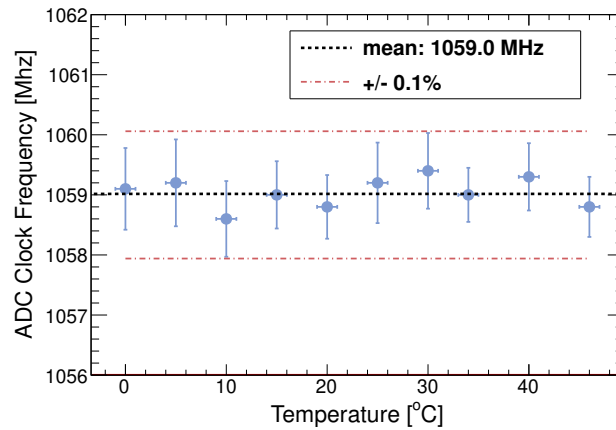


Figure 8: Ring oscillator clock stability over temperature. This clock is stabilized with a servo-control algorithm in the FPGA that adjusts the DAC oscillator voltage controls. With this feedback, the ring oscillator frequency is held within 0.1% of the nominal 1.059 GHz over the tested temperature range.

158 RMS cell-to-cell gain dispersion is $\sim 1\%$ over an 0.8 V range. Over this range, a single count-to-voltage LUT
 159 per channel may be sufficient. To effectively use the entire PSEC4 DC dynamic range, a count-to-voltage
 160 conversion LUT should be implemented for each individual cell.

161 3.1.1. Temperature Dependance

162 The ring oscillator ADC clock is the most temperature sensitive circuit and is servo-controlled using the
 163 FPGA to better than 0.1% over a wide temperature range as shown in Figure 8. The ADC clock frequency

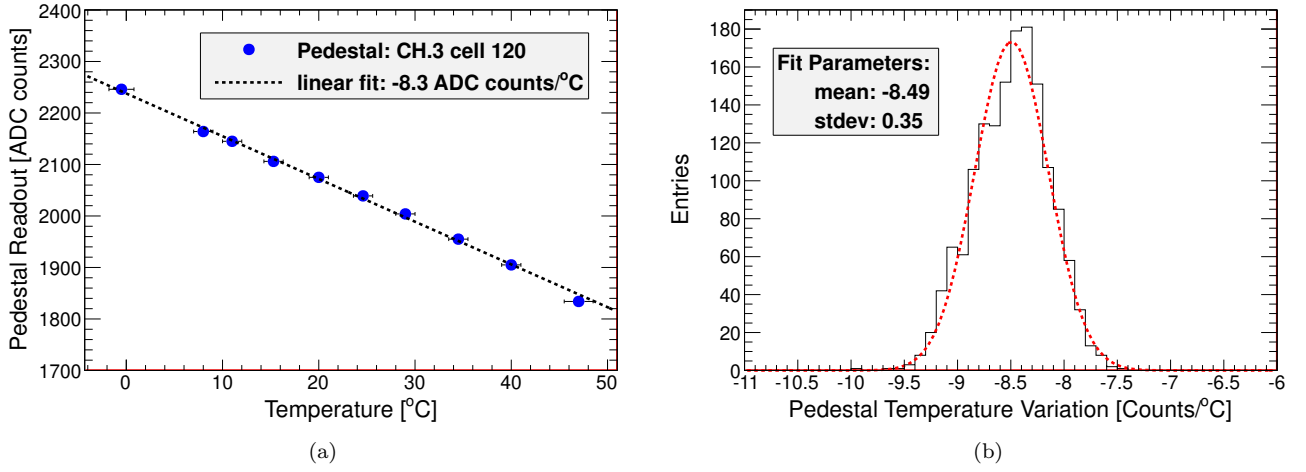


Figure 9: (a) Temperature dependence of the pedestal level of a single cell. The data are consistent with a linear change in pedestal level over temperature. (b) Distribution of pedestal-temperature variations over entire chip. The pedestal-temperature trend is consistent to 4% over all 1536 cells of a PSEC4 chip.

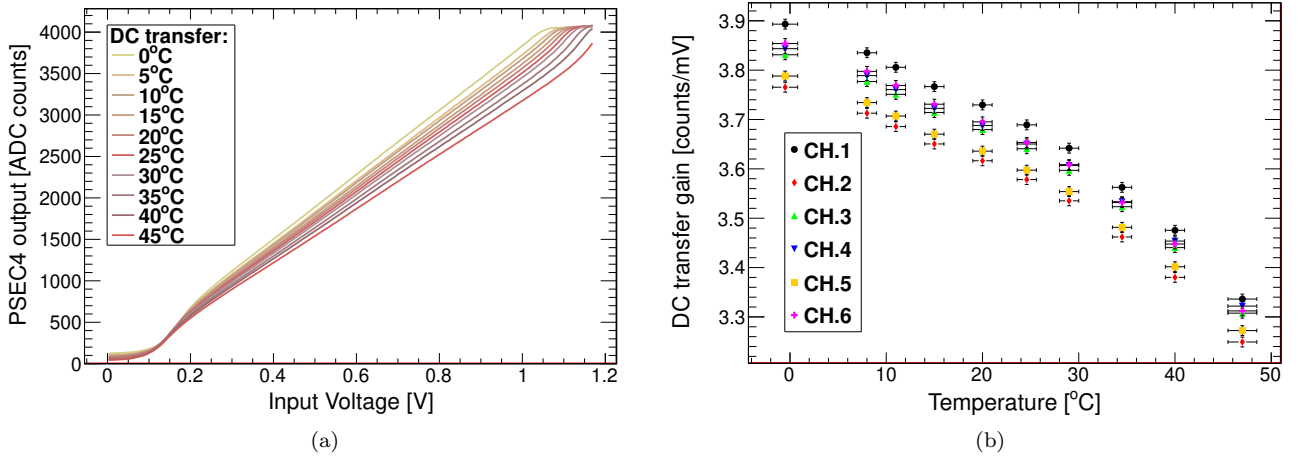


Figure 10: (a) Average DC response of a single PSEC4 channel over a temperature range of 0°C to 45°C. (b) The extracted DC transfer gains as a function of temperature for all channels.

164 was measured using 50k events at each temperature. Other temperature sensitive circuitry, including the
 165 chip-global ramp generator, are not feedback controlled.

166 The mid-range cell pedestal temperature dependence is shown in Figure 9a. Pedestal levels are computed
 167 for each cell by recording the average ADC baseline over several readouts. The pedestal variation is consistent
 168 with a linear trend of ~ 8.5 ADC counts/°C. This trend is common to all cells in PSEC4 as shown in Figure 9b.
 169 A simple event baseline subtraction can correct for this effect with 4% accuracy.

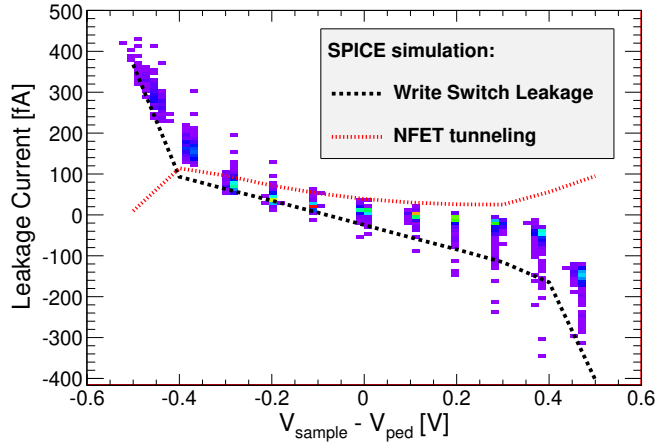


Figure 11: PSEC4 sample cell leakage measured at room temperature. The measured leakage is shown by the histogrammed data points. Results from a $0.13 \mu\text{m}$ CMOS SPICE simulation are also included. The simulation shows the leakage current contributions from 1) sub-threshold conduction through the disengaged write switch; and 2) gate-oxide tunneling from the NFET in the input stage of the comparator.

170 The count-to-voltage transfer also shows temperature variation due to changes in the ADC ramp slope.
 171 The average DC transfer curves at different temperatures are shown in Figure 10a. The count-per-voltage
 172 gain is extracted from a fit to the linear region of the DC transfer curve and is plotted in Figure 10b. Since
 173 the ADC ramp is common to all channels, the average DC transfer gains of all channels are observed to have
 174 the same temperature dependence. To mitigate this effect, a feedback loop that serves the ramp current
 175 source could be implemented.

176 3.2. Sample Leakage

177 When triggered, the write switch on each cell is opened and the sampled voltage is held at high impedance
 178 on the 20 fF capacitor (Fig. 3). Two charge leakage pathways are present: 1) sub-threshold conduction
 179 through the write switch formed by transistors T1 and T2; and 2) gate-oxide tunneling through the NFET
 180 at the comparator input. The observable leakage current is the sum of these two effects.

181 To measure the leakage current, a 300 ns wide, variable-level pulse was sent to a single PSEC4 channel.
 182 Since the sampling window is 25 ns, each SCA cell sampled the transient level. After triggering, the sampled
 183 transient voltage was repeatedly digitized at 1 ms intervals and the change in voltage on the capacitor was
 184 recorded over a 10 ms storage-time.

185 The room temperature PSEC4 leakage current as a function of input voltage over the full 1 V dynamic
 186 range is shown in Figure 11. A pedestal level of $V_{DD}/2 = 0.6 \text{ V}$ was set at the input. The measured leakage
 187 is shown in the 2-D histogram. A large spread (RMS $\sim 70 \text{ fA}$) is seen at each voltage level. Results from

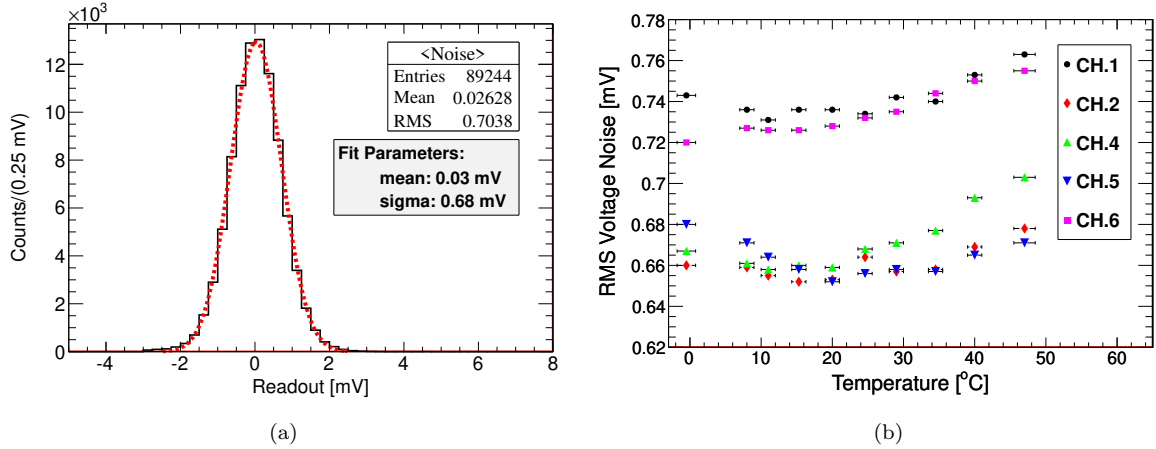


Figure 12: (a) A PSEC4 baseline readout showing the electronic noise. The data are recorded from single channel after offset correction. The RMS value of $\sim 700 \mu\text{V}$ is representative of the electronics noise on all channels. (b) Channel RMS noise measured over temperature.

188 a $0.13 \mu\text{m}$ CMOS SPICE simulation show that the write-switch leakage is the dominant pathway. A small
 189 amount ($\leq 100 \text{ fA}$) of NFET gate-oxide tunneling is also consistent with the data.

190 In normal operation, the ADC is started immediately after a trigger is registered. In this case, the analog
 191 voltage hold time is limited to the ADC conversion time. Assuming a constant current, the leakage-induced
 192 voltage change is given by

$$\Delta V = \frac{I_{leakage} \Delta t}{C_{sample}} \quad (3)$$

193 where Δt is the ADC conversion time. With the maximum leakage current of $\pm 500 \text{ fA}$ and a conversion
 194 time of $4 \mu\text{s}$, ΔV is $\pm 100 \mu\text{V}$. This value is at least $5\times$ lower than the electronics noise.

195 3.3. Noise

196 After fixed-pattern pedestal correction and event-by-event baseline subtraction, which removes low-
 197 frequency noise contributions, the PSEC4 electronic noise is measured to be $\sim 700 \mu\text{V}$ RMS on all channels
 198 as shown in Figure 12a. The noise level is consistently sub-mV over a $\pm 20^\circ\text{C}$ temperature range around
 199 room temperature. Above $\sim 20^\circ\text{C}$, the electronics noise increases with temperature, which is consistent
 200 with the thermal noise expectation of $\sqrt{k_B T / C}$ (Figure 12b). The noise figure is dominated by broadband
 201 thermal noise on the 20 fF sampling capacitor, which contributes $450 \mu\text{V}$ (RMS 60 electrons) at 300 K.
 202 Other noise sources include the ADC ramp generator and comparator. The noise corresponds to roughly 3
 203 least significant bits (LSBs), reducing the DC RMS dynamic range to 10.5 bits over the signal voltage range.

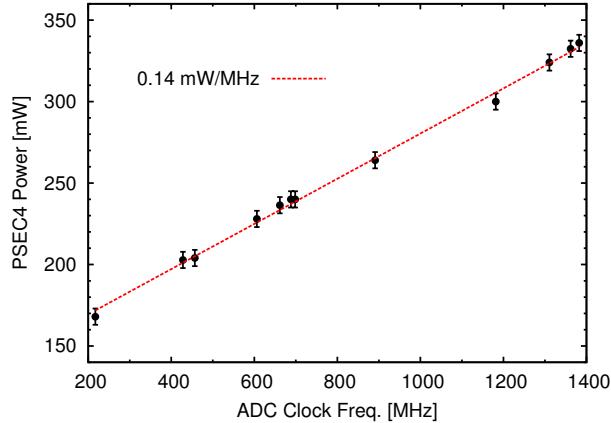


Figure 13: Total PSEC4 power as a function of the ADC clock rate. Clock rates between 200 MHz and 1.4 GHz can be selected based on the power budget and targeted ADC speed and resolution. When the ADC is not running, the quiescent (continuous sampling) power consumption is ~ 40 mW per chip.

204 3.4. Power

205 The power consumption is dominated by the ADC, which simultaneously clocks 1536 ripple counters and
 206 several hundred large digital buffers at up to 1.4 GHz. The total power draw per chip as a function of ADC
 207 clock rate is shown in Figure 13. To reduce the steady state power consumption and to separate the chip's
 208 digital processes from the analog sampling, the ADC is run only after a trigger is sent to the chip. Without
 209 a trigger, the quiescent power consumption is ~ 40 mW per chip, including the locked VCDL sampling at
 210 10.24 GSa/s and the current biases of all the comparators.

211 Initiating the ADC with a clock rate of 1 GHz causes the power draw to increase from 40 mW to
 212 300 mW within a few nanoseconds. To mitigate high-frequency power supply fluctuations when switching
 213 on the ADC, several 'large' (2 pF) decoupling capacitors were placed on-chip near the ADC. These capacitors,
 214 in addition with the close-proximity evaluation board decoupling capacitors (~ 0.1 - $10 \mu\text{F}$), prevent power
 215 supply transients from impairing chip performance.

216 At the maximum PSEC4 sustained trigger rate of 50 kHz, in which the ADC is running 20% of the time,
 217 a maximum average power of 100 mW is drawn per chip.

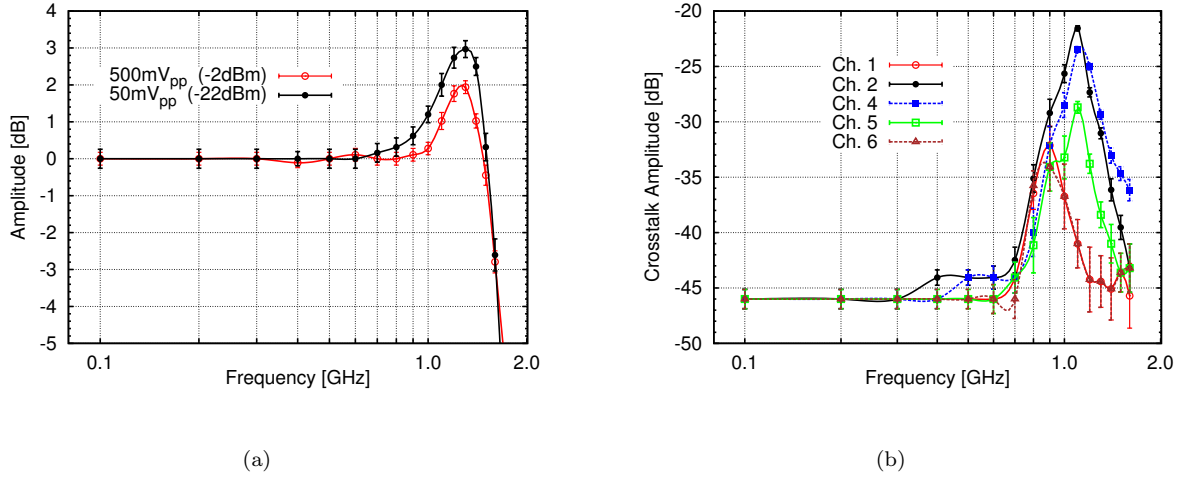


Figure 14: (a) PSEC4 frequency response. The -3 dB analog bandwidth is 1.5 GHz. The positive resonance above 1 GHz is due to bondwire inductance of the signal wires in the chip package. Similar responses are shown for large and small sinusoidal inputs. (b) Channel-to-channel crosstalk as a function of frequency. Channel 3 was driven with a -2 dBm sinusoidal input. Adjacent channels see a maximum of -20 dB crosstalk at 1.1 GHz. The electronic noise floor is -50 dB for reference.

218 3.5. Frequency Response

219 The target analog bandwidth for the PSEC4 design was ≥ 1 GHz. The bandwidth is limited by the
 220 parasitic input capacitance (C_{in}), which drops the input impedance at high frequencies⁶ as

$$|Z_{in}| = \frac{R_{term}}{\sqrt{1 + \omega^2 R_{term} C_{in}}} \quad (4)$$

221 where R_{term} is an external 50 Ω termination resistor. Accordingly, the expected half-power bandwidth is
 222 given by:

$$f_{3dB} = \frac{1}{2\pi R_{term} C_{in}} \quad (5)$$

223 The extracted C_{in} from post-layout studies was ~ 2 pF, projecting a -3 dB bandwidth of 1.5 GHz which
 224 corresponds to the measured value shown in Figure 14a. The chip package-to-die bondwire inductance gives
 225 a resonance in the response above 1 GHz that distorts signal content at these frequencies. An external filter
 226 may be added to flatten the response.

227 The error bars correspond to the measurement procedure, in which several thousand sine waves are

⁶This ignores negligible contributions to the impedance due to the sampling cell input coupling. The write switch on-resistance (≤ 4 k Ω over the full dynamic range) and the 20 fF sampling capacitance introduce a pole at ≥ 2 GHz.

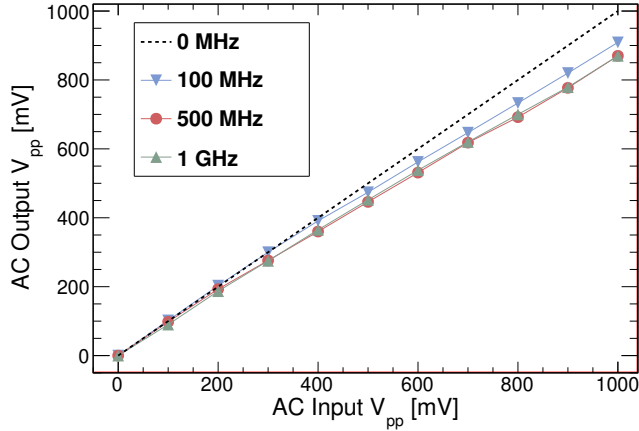


Figure 15: AC response of a single channel. The PSEC4 data were converted to voltage using the DC linearity LUT as shown in Fig. 6. Saturation of the AC signals is observed for all frequencies, most clearly above 500 mV_{pp}

228 recorded at each frequency and histogrammed. The histogram bins with the maximum values are at the
 229 high and low peaks of the PSEC4-digitized sine wave. These peaks are fitted with a Gaussian function, from
 230 which the mean sine wave amplitude and measurement error (σ from fits) is extracted

231 The measured channel-to-channel crosstalk is -25 dB below 1 GHz for all channels as shown in Figure 14b.
 232 For frequencies less than 700 MHz, this drops to better than -40 dB. The primary crosstalk mechanism is
 233 thought to be the mutual inductance between signal bondwires in the chip package. High frequency substrate
 234 coupling on the chip or crosstalk between input traces on the PSEC4 evaluation board may also contribute.

235 3.5.1. AC linearity

236 The PSEC4 response to sinusoidal signals of varying magnitude is shown in Figure 15. The AC signals
 237 were calibrated using the DC transfer count-to-voltage LUT (Figure 6). Saturation is observed for signals
 238 as low as 100 MHz ($\sim 9\%$ above V_{pp} of 500 mV) and this effect becomes constant for frequencies above
 239 500 MHz ($\sim 15\%$ above V_{pp} of 500 mV).

240 This AC saturation effectively reduces the PSEC4 ADC resolution. With a DC calibration, it was shown
 241 that 10.5 bits effectively covered a 1 V dynamic range including electronics noise. At 100 MHz, the resolution
 242 drops to ~ 10.35 bits. For signals up to 1 GHz, the effective resolution is 10.3 bits. Additionally, an AC
 243 count-to-voltage conversion calibration LUT can be used for correct for this saturation.

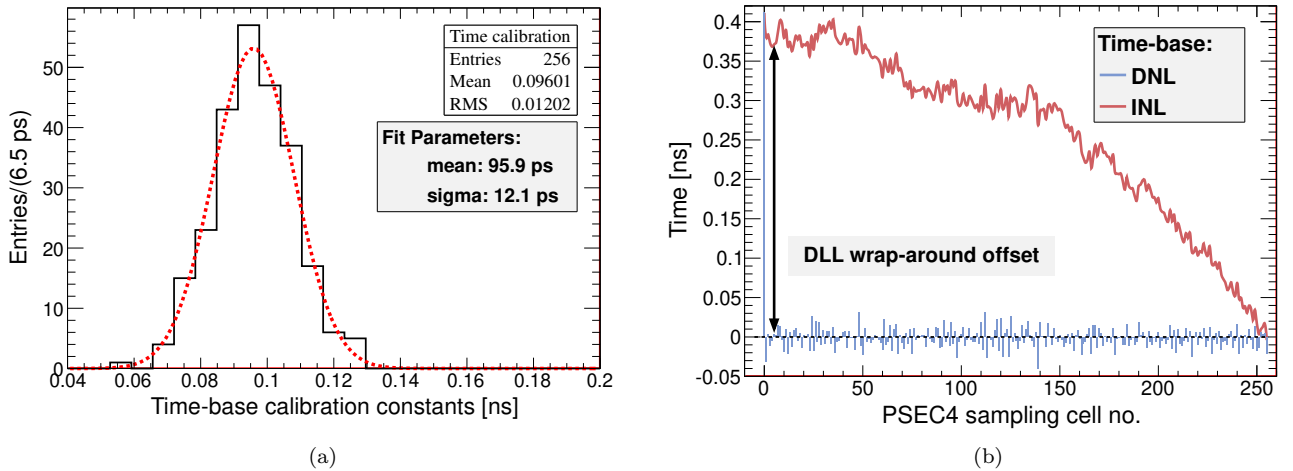


Figure 16: (a) A histogram of the extracted time-base calibration constants (Δt). These values are calculated using the zero-crossing technique and are used to correct the sampling time-base of the PSEC4 chip. (b) The differential (DNL) and integral non-linearity (INL) of the PSEC4 time-base. The extracted Δt 's are compared to an ideal linear time-base with equal time-steps per sample point. The large time-step at the first sample bin is caused by a fixed DLL latency when wrapping the sampling from the last cell to the first.

244 3.6. Sampling Calibration

245 For precision waveform feature extraction, both the overall time-base of the VCDL and the cell-to-cell
 246 time step variations must be calibrated. With the rate-locking DLL, the overall PSEC4 sampling time
 247 base is stably servo-controlled at a default rate of 10.24 GSa/s. The time-base calibration of the individual
 248 256 delay stages, which vary due to cell-to-cell transistor size mismatches in the VCDL, is the next task.
 249 Since this is a fixed-pattern variation, the time-base calibration is typically a one-time measurement.

250 The brute force ‘zero-crossing’ time-base calibration method is employed [25]. This technique counts
 251 the number of times a sine wave input crosses zero voltage at each sample cell. With enough statistics, the
 252 corrected time per cell is extracted from the number of zero-crossings (N_{zeros}) using

$$\langle \Delta t \rangle = \frac{T_{input} \langle N_{zeros} \rangle}{2 N_{events}} \quad (6)$$

253 where T_{input} is the period of the input and N_{events} is the number of digitized sine waveforms. A typical
 254 PSEC4 time-base calibration uses 10^6 recorded events of 400 MHz sinusoids.

255 The variation of the time-base sampling steps is $\sim 13\%$ as shown in Figure 16a. Due to a relatively large
 256 time step at the first cell, the average sampling rate over the remaining VCDL cells is ~ 10.4 GSa/s, slightly
 257 higher than the nominal rate. With the servo-locking DLL the INL is constrained to be zero at the last cell.

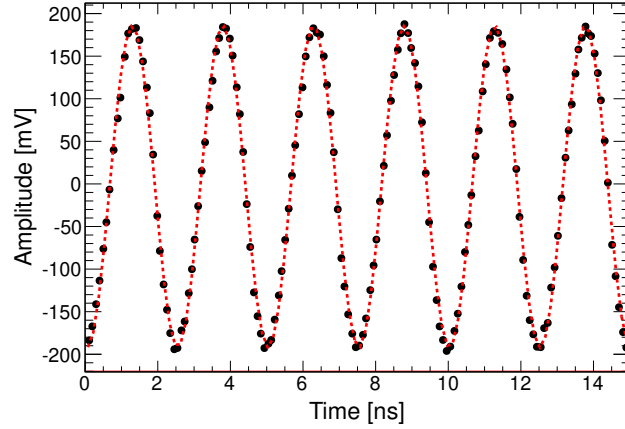


Figure 17: A 10.24 GSa/s capture of a 400 MHz sine input is shown (black dots) after a channel-only linearity correction and time-base calibration. A fit (red dotted line) is applied to the data.

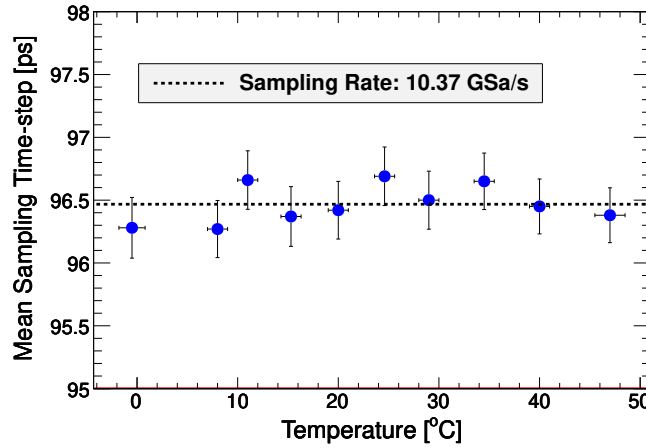


Figure 18: Mean time-base step as measured over a temperature range -1°C to 46°C . The sampling rate is held constant over temperature with the on-chip DLL.

258 A digitized 400 MHz sine wave is shown in Figure 17 after applying the time-base calibration constants.

259 The non-linearity of the PSEC4 time-base is shown in Figure 16b. Each bin in the plot is indicative of
 260 the time-base step between the binned cell and its preceding neighbor cell. The relatively large DNL in the
 261 first bin, which corresponds to the delay between the last (cell 256) and first sample cells, is caused by a
 262 fixed DLL latency when wrapping the sampling from the last cell to the first.

263 The mean sampling rate is shown in Figure 18 to be uniform over temperature. This is an expected
 264 feature of the on-chip DLL. Fifty-thousand events were recorded at each temperature point and the zero
 265 crossing algorithm was run on each dataset. No temperature dependence is observed.

266 3.7. Waveform Timing

267 The effective timing resolution of a single measurement is calculated by waveform feature extraction after
268 linearity and time-base calibration. A $0.5 V_{pp}$, 1.25 ns FWHM Gaussian pulse was created using a 10 GSa/s
269 arbitrary waveform generator (Tektronix AWG5104). The output of the AWG was sent to 2 channels of
270 the ASIC using a broadband-RF 50/50 splitter (Mini-Circuits ZFRSC-42). This pulse, as recorded by a
271 channel of PSEC4, is shown in Figure 19a. A least-squares Gaussian functional fit is performed to the
272 leading edge of the pulse. The pulse times from both channels are extracted from the fit and are subtracted
273 on an event-by-event basis.

274 The timing resolution measurements are shown in Figure 19b, in which the pulses are injected asyn-
275 chronously to two channels of PSEC4. In this measurement, the two pulses were delayed relative to one-
276 another and the waveforms were captured uniformly across the 25 ns PSEC4 sampling buffer. Ten-thousand
277 events were recorded at each delay stage. The time difference resolution was extracted by the waveform
278 fitting procedure shown in Figure 19a, before and after applying the time-base calibration to both channels.
279 A consistent timing resolution between 4 and 7 ps was measured over a 20 ns span of pulse separation.

280 The fitting procedure that was used to extract the timing information exposes the non-uniformity of the
281 PSEC4 time-base. With the uncalibrated time-base data, the 2-channel timing resolution is found to be
282 ~ 30 ps for pulse delays greater than 5 ns.

283 The timing resolution measured as a function of pulse location in the PSEC4 buffer is shown in Figure 20.
284 This 2-channel measurement was performed using two pulses at identical times. The resolution is observed
285 to degrade as the pulses are captured further into the PSEC4 sample buffer.

286 3.8. Performance Summary

287 The performance and key architecture parameters of PSEC4 are summarized in Table 1.

288 4. Conclusions

289 We have described the architecture and performance of the PSEC4 waveform digitizing ASIC. The ad-
290 vantages of implementing waveform sampling IC design in a deeper sub-micron process are shown, with
291 measured sampling rates of up to 15 GSa/s and analog bandwidths of 1.5 GHz. Potential $0.13 \mu\text{m}$ de-
292 sign issues, such as leakage and dynamic range, were optimized and provide a 1 V dynamic range with
293 sub-mV electronics noise. After a one-time timebase calibration, it is possible to extract precision timing
294 measurements (~ 5 ps) when applying a rising-edge fit to the PSEC4 digitized waveform.

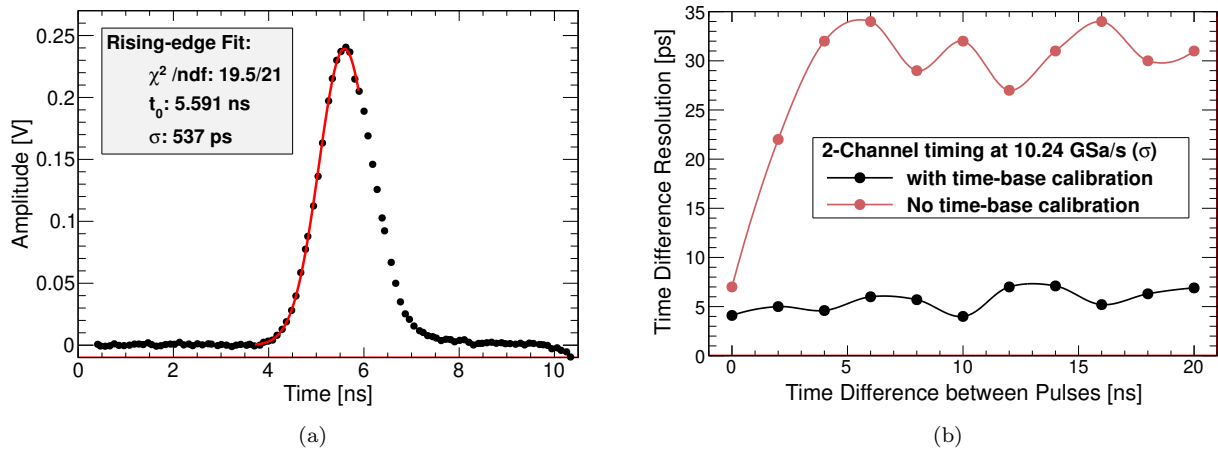


Figure 19: (a) An example PSEC4 digitized pulse (black dots) and waveform fit (red line) that was used for the timing resolution measurement. A 1.25 ns FWHM Gaussian pulse was split and injected into two channels of the chip. The waveform was captured at 10.24 GSa/s and is shown after applying the time-base calibration constants. (b) Two-channel time resolution from asynchronous pulse injection into PSEC4. The timing resolution as a function of pulse separation in the PSEC4 sampling buffer is shown.

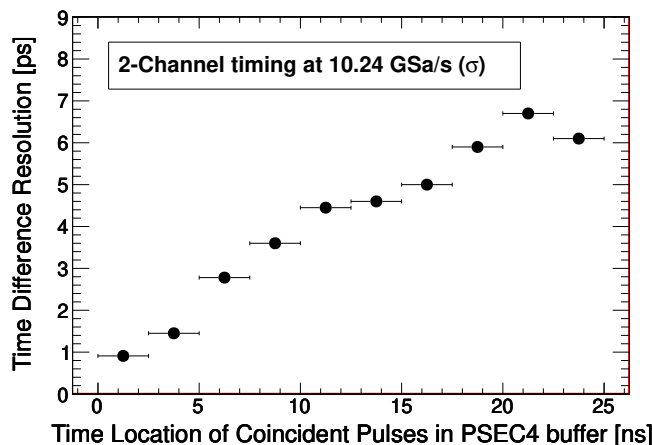


Figure 20: Timing resolution vs. pulse location in PSEC4 sampling buffer. This corresponds to the 2-channel coincidence timing, in which the pulses were not delayed with respect to one another.

295 5. Acknowledgements

296 We thank Mircea Bogdan, Fukun Tang, Mark Zaskowski, and Mary Heintz for their strong support in the
 297 Electronics Development Group of the Enrico Fermi Institute. Stefan Ritt, Eric Delagnes, and Dominique
 298 Breton provided invaluable guidance and advice on SCA chips. We thank Kostas Kloukinas and the MOSIS
 299 educational program for support and advice on the 0.13 μ m CMOS process and project submissions

300 This work is supported by the Department of Energy, Contract Nos. DE-AC02-06CH11357 and DE-

Table 1: PSEC4 architecture parameters and measured performance results.

Parameter	Value	Comment
Channels	6	die size constraint
Sampling Rate	4-15 GSa/s	servo-locked on-chip
Samples/channel	256	249 samples effective
Recording Buffer Time	25 ns	at 10.24 GSa/s
Analog Bandwidth	1.5 GHz	
Crosstalk	7%	max. over bandwidth
	<1%	typical for signals <800 MHz
Noise	700 μ V	RMS (typical). RF-shielded enclosure. After calibration.
DC RMS Dynamic Range	10.5 bits	12 bits logged
Signal Voltage Range	1 V	after linearity correction
ADC conversion time	4 μ s	max. 12 bits logged at 1 GHz clock speed
	250 ns	min. 8-bits logged at 1 GHz
ADC clock speed	1.4 GHz	max.
Readout time	0.8 n μ s	n is number of 64-cell blocks to read ($n = 24$ for entire chip)
Sustained Trigger Rate	50 kHz	max. per chip. Limited by [ADC time + Readout time] ⁻¹
Power Consumption	100 mW	max. average power
Core Voltage	1.2 V	0.13 μ m CMOS standard

301 SC0008172 , and the National Science Foundation, Grant No. PHY-106 601 4.

302 References

- 303 [1] J.-F. Genat, G. Varner, F. Tang, H.J. Frisch, “Signal Processing for Pico-second Resolution Timing Measurements”, Nucl.
304 Instr. Meth. A 607 (2009) 387-393.
- 305 [2] D. Breton, E. Delagnes, J. Maalmi, K. Nishimura, L.L. Ruckman, G. Varner, J. Va’vra, “High Resolution Photon Timing
306 with MCP-PMTs: A Comparison of Commercial Constant Fraction Discriminator (CFD) with ASIC-based waveform
307 digitizers TARGET and WaveCatcher”, Nucl. Instr. Meth A 629 (2011) 123-132.
- 308 [3] S. Kleinfelder, “Development of a Switched Capacitor Based Multi-Channel Transient Waveform Recording Integrated
309 Circuit”, IEEE Trans. Nucl. Sci. 35, (1988) 151-154.
- 310 [4] G. Haller, B. Wooley, “A 700 MHz Switched Capacitor Analog Waveform Sampling Circuit”, SLAC-PUB-6414 (1993).
- 311 [5] S. Ritt, “Gigahertz Waveform Sampling: An Overview and Outlook”, 12th Pisa Meeting on Advanced Detectors, 23d May
312 2012.
- 313 [6] G.S. Varner, L.L. Ruckman, J.W. Nam, R.J. Nichol, J. Cao, P.W. Gorham, M. Wilcox, “The Large Analog Bandwidth
314 Recorder and Digitizer With Ordered Readout (LABRADOR) ASIC”, Nucl. Instr. Meth. A 583 (2007) 447-460.
- 315 [7] E. Delagnes, Y. Degerli, P. Goret, P. Nayman, F. Toussnel, P. Vincent, “SAM: A new GHz sampling ASIC for the
316 H.E.S.S.-II Front-End Electronics”, Nucl. Instr. Meth. A 567 (2006) 21-26.
- 317 [8] K. Bechtol, S. Funk, A. Okumura, L. Ruckman, A. Simons, H. Tajima, J. Vandenbroucke, G. Varner, “TARGET: A
318 Multi-Channel Digitizer Chip for Very-High-Energy Gamma-Ray Telescopes”, J. Astroparticle Physics 36 (2012) 156-165.
- 319 [9] S. Kleinfelder, “Gigahertz Waveform Sampling and Digitization Circuit Design and Implementation”, IEEE Trans. Nucl.
320 Sci. 50, (2003) 955-962.

- 321 [10] G.S. Varner, P. Gorham, J. Cao, "Monolithic Multi-Channel GSa/s Transient Waveform Recorder for Measuring Radio
322 Emissions from High Energy Particle Cascades", Proc. SPIE Int. Soc. Opt. Eng 4858 (2003) 31.
- 323 [11] C. Broennimann, R. Horisberger, R. Schnyder, "The Domino Sampling Chip: A 1.2 GHz Waveform Sampling CMOS
324 Chip", Nucl. Instr. Meth. A 420 (1999) 264-269.
- 325 [12] S. Ritt, "The DRS Chip: Cheap Waveform Digitization in the GHz Range", Nucl. Instr. Meth. A 518 (2004) 470-471.
- 326 [13] J. Milnes, J. Howorth, "Picosecond Time Response Characteristics of Micro-channel Plate PMT Detectors", SPIE USE,
327 V. 8 5580 (2004) 89-100.
- 328 [14] B. Adams, A. Elagin, H. Frisch, R. Obaid, E. Oberla, A. Vostrikov, R. Wagner, M. Wetstein, "Measurements of the Gain,
329 Time Resolution, and Spatial Resolution of a 20x20 cm² MCP-based Picosecond Photo-Detector", Submitted to Nucl.
330 Instr. Meth. A (2013).
- 331 [15] P. Eraerds, M. Legré, A. Rochas, H. Zbinden, N. Gisin, "SiPM for fast Photon-Counting and Multiphoton Detection",
332 Optics Express, Vol. 15 (2007) 14539-14549.
- 333 [16] S. Ritt, "The Role of Analog Bandwidth and S/N in Timing", talk at *The Factors that Limit Timing Resolution in*
334 *Photodetectors*, <http://psec.uchicago.edu/workshops/fast_timing_conf.2011/>, University of Chicago, Apr 2011.
- 335 [17] R.H. Dennard, F. H. Gaennslen, H. N. Yu, V.L Rideout, E. Bassous, A.R. LeBlanc, "Design of Ion-Implemented MOS-
336 FETs with Very Small Physical Dimensions," IEEE J. Solid-State Circuits SC-9 (1974) 256-268.
- 337 [18] Y. Taur et. al., "CMOS Scaling into the Nanometer Regime", Proc. IEEE. Vol. 85, No. 4, (1997) 486-504.
- 338 [19] IBM Corporation, "CMRF8SF Model Reference Guide", V.1.4.0.10 (2008).
- 339 [20] The MOSIS Service. Wafer Electrical Test Data and SPICE Model Parameters. Run: V18B. Available on-line (accessed
340 4 Feb. 2013): <<http://www.mosis.com/pages/Technical/Testdata/ibm-013-prm>>
- 341 [21] E. Oberla, H. Grabas, M. Bogdan, H. Frisch, J.-F. Genat, K. Nishimura, G. Varner, A. Wong, "A 4-Channel Waveform
342 Sampling ASIC in 0.13 μm CMOS for Front-End Readout of Large-Area Micro-Channel Plate Detectors", Physics Procedia
343 37 (2012) 1690-1698.
- 344 [22] M. Cooney, M. Andrew, K. Nishimura, L. Ruckman, G. Varner, H. Grabas, E. Oberla, J.-F. Genat, "Multipurpose
345 Test Structures and Process Characterization using 0.13 μm CMOS: The CHAMP ASIC", Physics Procedia 37 (2012)
346 1699-1706.
- 347 [23] H. Chang et al., "A Wide-Range Delay-Locked Loop With a Fixed Latency of One Clock Cycle", IEEE J. Solid-State
348 Circuits 37 (2002) 1021-1027.
- 349 [24] O. Milgrome, S. Kleinfelder, M. Levi, "A 12 Bit Analog to Digital Converter for VLSI Applications in Nuclear Science",
350 IEEE Trans. Nucl. Sci. 39, (1992) 771-775.
- 351 [25] K. Nishimura, A. Romero-Wolf, "A Correlation-Based Timing Calibration & Diagnostic Technique for Fast Digitization
352 ASICs", Physics Procedia 37 (2012) 1707-1714.